# RESPONSE OF THE MARTIAN UPPER ATMOSPHERE TO LOWER ATMOSPHERIC DUST STORMS: GCM STUDY

**A. S. Medvedev**, *Max Planck Institute for Solar System Research, Katlenburg-Lindau, Germany (medvedev@ mps.mpg.de)*, **E. Yiğit**, *George Mason University, Fairfax, USA,* **T. Kuroda**, *Tohoku University, Sendai, Japan,* **P. Hartogh**, *Max Planck Institute for Solar System Research, Katlenburg-Lindau, Germany*.

**Introduction:**

Global-scale effects of dust storms in the lower atmosphere of Mars are numerous. This presentation addresses the less studied aspect of dust storms—their manifestation and consequences in the upper atmosphere. The most comprehensive observational data set to date of upper atmospheric densities during dust storms was presented by *Withers and Pratt* [2013]. We use the MPI Martian General Circulation Model (MGCM) extending from the surface to the lower thermosphere (~150-160 km) to simulate the atmosphere during the equinoctial and solstitial major dust storms occurred in Martian years 25 and 28 (MY25 and MY28), correspondingly.

**Martian GCM:**

The MPI MGCM has recently been described in [*Medvedev et al.,* 2011; *Medvedev and Yiğit,* 2012]. It is based on a spectral dynamical core, and includes the physical parameterizations from the previous versions of this GCM [*Hartogh et al.*, 2005; Medvedev *and Hartogh*, 2007]. The vertical domain extends to pressure $p = 3.6 \times 10^{-6}$ Pa (approximately 150–160 km), and is represented by 67 hybrid levels, which are terrain-following near the surface, and pressure-based in the upper atmosphere. The presented simulations have been performed using a triangular spectral truncation T21.

The model accounts for the radiative transfer in the gaseous $CO_2$: LTE in the lower atmosphere, and non-LTE above 60-70 km. In the upper atmosphere, heating due to absorption of solar UV and EUV radiation by $CO_2$ molecules is calculated. Heating and cooling due to absorption, emission, and scattering by atmospheric dust are computed with the scheme of *Nakajima and Tanaka* [1986]. Vertical profiles of dust mixing ratio, $Q$, were prescribed using the revised version of the Conrath analytical formula, which accounts for the observations that aerosols usually extend higher in the equatorial zone, decay more abruptly toward the poles, and tend to penetrate higher when its total amount increases.

The GCM was interactively coupled with the spectral nonlinear gravity wave (GW) parameterization of *Yiğit et al.* [2008]. It calculates the vertical propagation of individual subgrid-scale harmonics (with the characteristic horizontal wavelength $\lambda_H$=300 km) from the source level in the lower atmosphere ($p$ = 260 Pa, ~8 km) accounts for refraction, nonlinear breaking/saturation, and dissipation by molecular viscosity and thermal conduction. It computes the momentum deposition ("drag") and heating/cooling rates. The source spectrum was approximated by 28 harmonics with horizontal phase velocities $|c|$ < 60 m/s aligned along the direction of the local wind.

**Scenarios of dust storms:**

To study the response of the atmosphere at two distinctive seasons, two particular major planet-encircling storms were chosen. One occurred around the Martian equinox (MY25), the other around the solstice (MY28). The corresponding scenarios in the form of zonally averaged latitude-time distributions of the total dust optical depth in IR from the MGS-TES and MEX-PFS are shown in Figure 1.

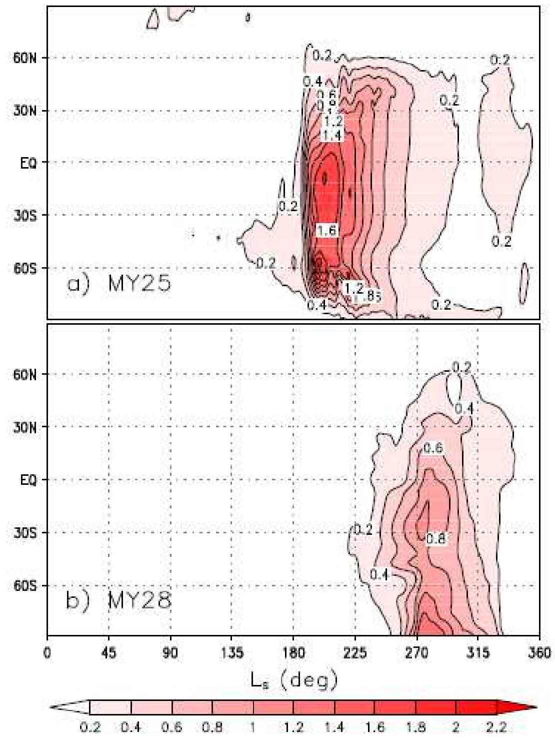


**Figure 1:** The observed dust total optical depth (in IR) during a) MY25 (31 May 2000 to 17 April 2002) and b) MY28 (21 January 2006 to 18 Dec 2007).

**Equinoctial dust storm:**

The results of simulations are presented for the peak period of the storm. All shown fields are the 17 sols averaged model output corresponding to the interval between $L_S$ =190 and $200^0$. We performed two runs for the MY25 dust scenario: with and without GWs, and compared them with the simulations for low dust conditions ($\tau$=0.2 in the visible). Figures 2a and 2b demonstrate the changes produced by the dust storm if no GWs were accounted for. Figures 2c and 2d are the same, but with the GW scheme turned on. Color shadings show temperature differences between the MY25 run and the low dust scenario. One can see a commonality in the simulated atmospheric temperature. The simulated lower atmospheric temperature increased by over 30 K due to enhanced absorption of solar radiation by dust particles, and the near-surface temperature dropped by 10 to 15 K owing to fewer solar energy penetrating the opaque atmosphere.

There is the unexpectedly strong cooling of the middle and upper atmosphere (above ~70–80 km, pressures below 0.5–0.1 Pa) away from North Pole. The temperature above the mesopause drops by up to –30 K, that is, by the same amount as it rises in the lower atmosphere, even though it is not directly affected by the dust storm. Note that this cooling is produced in both simulations (with and without GWs). This can indicate that the effect is not directly controlled by the parameterized subgrid-scale waves.

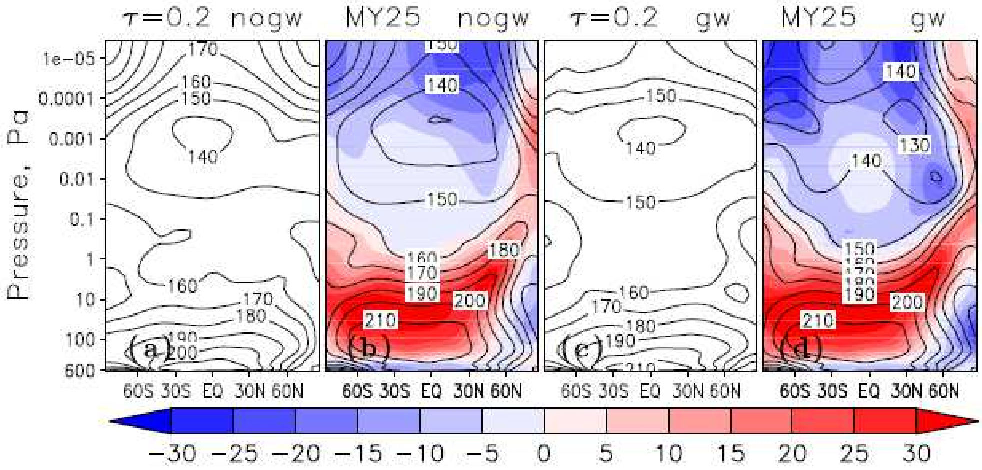


**Figure 2:** Mean zonal temperature averaged over *Ls* = 190–$200^0$ (contours): (a) for the low dust conditions ($\tau$= 0.2) and without the GW scheme, (b) for the MY25 dust storm and without GW scheme, (c) for $\tau$ = 0.2 but with the GW scheme included, and (d) for the MY25 dust storm and with the GW scheme. Shaded is the temperature difference between the corresponding "dust storm" and "low dust" simulations: without GW scheme (Figure 2b) and with GW parameterization included (Figure 2d).

**Solstitial dust storm:**

Simulated zonal mean temperature in Figure 3 represents the model output averaged over 15 sols at the midst of the MY28 storm approximately between *Ls* = 270 and $280^0$.

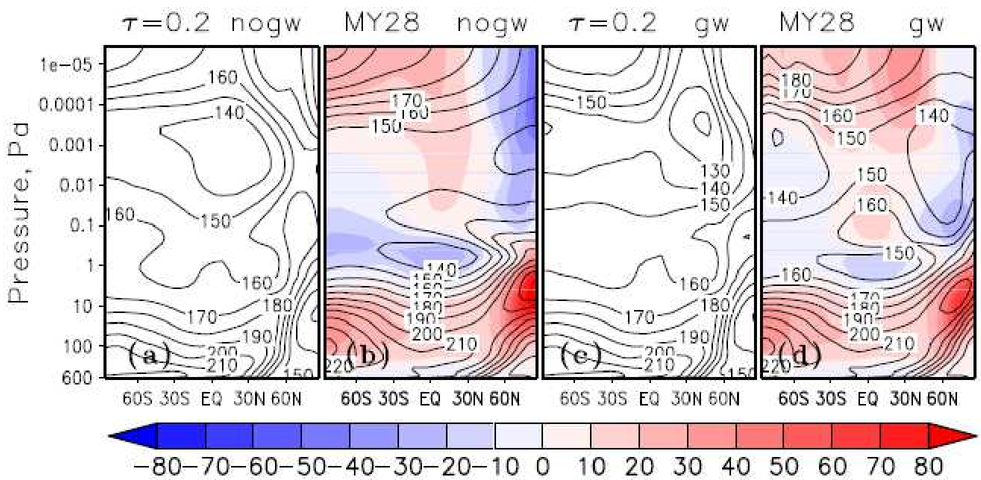


**Figure 3** Same as in Figure 2 but for the MY28 dust storm at *Ls*=270-$280^0$.

Although the absolute values of temperature above ~0.1 Pa differ in the simulations with and without parameterized GWs as in the equinoctial case, the effects of the dust storm are quite similar. The lower atmospheric temperature increased, in average, by 30–40 K and by 70–80 K over the winter pole below 1 Pa. The most notable of changes in the mesosphere and lower thermosphere are 20 to 30 K cooling above the temperature peak over the North Pole, 10 to 30 K cooling over the opposite pole that extends to ~100 km (0.01 Pa), and 20 to 30 K warmer temperatures in tropics and everywhere above ~110 km. Although the changes in the upper atmosphere during the storms of MY25 and MY28 are different, their magnitudes are almost the same as those in the lower atmosphere, where the increase of airborne aerosol took place. Temperature changes induced by the dust storm can be directly related to the adiabatic heating associated with the modified meridional circulation. The relative role of resolved and parameterized (GW) waves in altering the circulation will be discussed in the talk.

**Density changes:**

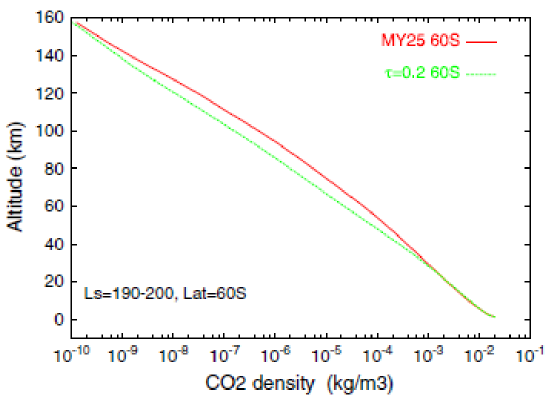


**Figure 4:** Zonal mean density profiles at $60^0$S from the simulations for the low dust conditions ($\tau$=0.2, green line) and for the MY25 storm (red) at *Ls*= 190–$200^0$.

*Withers and Pratt* [2013] presented observational evidences of upper atmospheric density enhancements during dust storms. On the other hand, *Forbes et al.* [2008] concluded that the 2001 storm "did not perceptibly influence exosphere temperature or density." Simulations presented in Figure 4 reconcile both observational conclusions, and demonstrate density enhancements in the lower thermosphere by a factor 2 to 3.

**Conclusions:**

Simulations with a Martian general circulation model (GCM) extending from the surface to the lower thermosphere (~160 km) show that wind and temperature in the upper atmosphere above 100 km respond to dust storms as intensively as in the lower atmosphere. These changes are the result of the altered meridional overturning circulation induced by resolved and unresolved waves. Atmospheric density during dust storms enhances in average by a factor of 2 to 3 in the mesosphere and lower thermosphere, which agrees well with observations.

**References:**

Forbes, J. M., F. G. Lemoine, S. L. Bruinsma, M. D. Smith, and X. Zhang (2008), Geophys. Res. Lett., 35, L01201, doi:10.1029/2007GL031904.

Hartogh, P., A. S. Medvedev, T. Kuroda, R. Saito, G. Villanueva, A. G. Feofilov, A. A. Kutepov, and U. Berger (2005), J. Geophys. Res., 110, E11008, doi:10.1029/2005JE002498.

Medvedev, A. S., and P. Hartogh (2007), Icarus, 186, 97–110.

Medvedev, A. S., and E. Yiğit (2012), Geophys. Res. Lett., 39, L05201, doi:10.1029/2012GL050852.

Medvedev, A. S., E. Yiğit, P. Hartogh, and E. Becker (2011), J. Geophys. Res., 116, doi:10.1029/2011JE003848.

Withers, P., R. Pratt (2013*), Icarus, 225*, 378–389.

Yiğit, E., A. D. Aylward, and A. S. Medvedev (2008), J. Geophys. Res., 113, doi:10.1029/2008JD010135.